MAGNETIC QUENCHING OF TURBULENT DIFFUSIVITY: RECONCILING MIXING-LENGTH THEORY ESTIMATES WITH KINEMATIC DYNAMO MODELS OF THE SOLAR CYCLE

Andrés Muñoz-Jaramillo[1,2], Dibyendu Nandy[3], and Petrus C. H. Martens[1,2]
[1] Department of Physics, Montana State University, Bozeman, MT 59717, USA; martens@solar.physics.montana.edu
[2] Harvard-Smithsonian Center for Astrophysics, Cambridge, MA 02138, USA; amunoz@cfa.harvard.edu
[3] Indian Institute for Science Education and Research, Kolkata, Mohampur 741252, West Bengal, India; dnandi@iiserkol.ac.in

ABSTRACT

The turbulent magnetic diffusivity in the solar convection zone is one of the most poorly constrained ingredients of mean-field dynamo models. This lack of constraint has previously led to controversy regarding the most appropriate set of parameters, as different assumptions on the value of turbulent diffusivity lead to radically different solar cycle predictions. Typically, the dynamo community uses double-step diffusivity profiles characterized by low values of diffusivity in the bulk of the convection zone. However, these low diffusivity values are not consistent with theoretical estimates based on mixing-length theory, which suggest much higher values for turbulent diffusivity. To make matters worse, kinematic dynamo simulations cannot yield sustainable magnetic cycles using these theoretical estimates. In this work, we show that magnetic cycles become viable if we combine the theoretically estimated diffusivity profile with magnetic quenching of the diffusivity. Furthermore, we find that the main features of this solution can be reproduced by a dynamo simulation using a prescribed (kinematic) diffusivity profile that is based on the spatiotemporal geometric average of the dynamically quenched diffusivity. This bridges the gap between dynamically quenched and kinematic dynamo models, supporting their usage as viable tools for understanding the solar magnetic cycle.

Key words: Sun: activity – Sun: dynamo – Sun: interior

Online-only material: color figures

1. INTRODUCTION

The solar magnetic cycle involves the recycling of the toroidal and poloidal components of the magnetic field, which are generated at spatially segregated source layers that must communicate with each other (see, e.g., Wilmot-Smith et al. 2006; Charbonneau 2010). This communication is mediated via magnetic flux transport, which in most kinematic solar dynamo models is achieved through diffusive and advective (i.e., by meridional circulation) transport of magnetic fields. The relative strength of turbulent diffusion and meridional circulation determines the regime in which the solar cycle operates, and this has far reaching implications for cycle memory and solar cycle predictions (Yeates et al. 2008; Nandy 2010). As shown in Yeates et al. (2008), different assumptions on the strength of turbulent diffusivity in the bulk of the solar convection zone (SCZ) lead to different predictions for the solar cycle (Dikpati et al. 2006; Choudhuri et al. 2007). Previously, this lack of constraint has led to controversy regarding what value of turbulent diffusivity is more appropriate and yields better solar-like solutions (Nandy & Choudhuri 2002; Dikpati et al. 2002; Chatterjee et al. 2004; Dikpati et al. 2005; Choudhuri et al. 2005). Currently, most dynamo modelers use double-step diffusivity profiles that are somewhat ad hoc and different from one another (see Figure 1; Rempel 2006a; Dikpati & Gilman 2007; Guerrero & de Gouveia Dal Pino 2007; Jouve & Brun 2007). There is, however, a way of theoretically estimating the radial dependence of magnetic diffusivity based on mixing-length theory (MLT; Prandtl 1925).

2. ORDER OF MAGNITUDE ESTIMATION

Going back to the derivation of the mean-field dynamo equations (after using the first-order smoothing approximation),

we find that the turbulent diffusivity coefficient becomes (Moffat 1978)

$$\eta = \frac{\tau}{3}\langle v^2 \rangle, \tag{1}$$

where τ is the eddy correlation time and v corresponds to the turbulent velocity field. In order to make an order of magnitude estimate we turn to MLT, which although not perfect has been found to be in general agreement with numerical simulations of turbulent convection (Chan & Sofia 1987; Abbett et al. 1997). More specifically we use the Solar Model S (Christensen-Dalsgaard et al. 1996), which is a comprehensive solar interior model used by GONG in all their helioseismic calculations. Among other quantities, this model estimates the mixing-length parameter α_p, the convective velocity v for different radii, and the necessary variables to calculate the pressure scale height H_p. In terms of those quantities the diffusivity becomes

$$\eta \sim \frac{1}{3}\alpha_p H_p v, \tag{2}$$

which we plot in Figure 1 (solid black line) and show how it compares to commonly used diffusivity profiles.

3. THE PROBLEM AND A POSSIBLE SOLUTION

It is evident that there is a major discrepancy between the theoretical estimate and the typical values used inside the convection zone (around two orders of magnitude difference). This creates a problem that is aggravated by the fact that dynamo models simply cannot operate under very strong diffusivities as suggested by MLT. A possible solution for this inconsistency resides in the back-reaction that strong magnetic fields have on velocity fields, which results in a suppression of turbulence and thus of turbulent magnetic diffusivity (Roberts & Soward 1975).
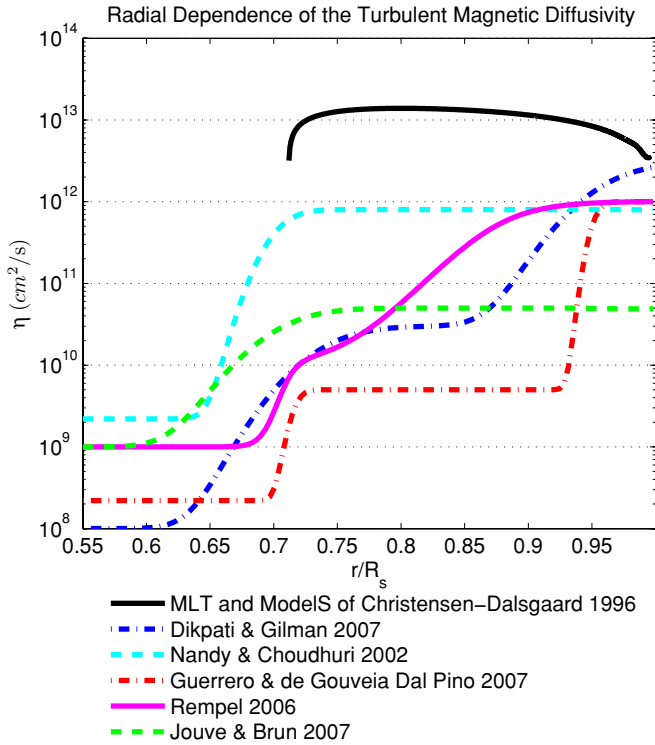
Figure 1. Different diffusivity profiles used in kinematic dynamo simulations. The solid black line corresponds to an estimate of turbulent diffusivity obtained by combining mixing-length theory (MLT) and the Solar Model S. The fact that viable solutions can be obtained with such a varied array of profiles has led to debates regarding which profile is more appropriate. Nevertheless, it is well known that kinematic dynamo simulations cannot yield viable solutions using the MLT estimate.

(A color version of this figure is available in the online journal.)

Magnetic "quenching" of the turbulent diffusivity has been studied before in different contexts by dynamo modelers: Rüdiger et al. (1994) studied quenching in the context of stellar and galactic geometries finding that the effect of quenching is more important in steady dynamos than in oscillating ones; Tobias (1996) studied quenching in the context of interface dynamos finding that quenching allows for the restriction of the magnetic field to a narrow layer in the interface between the convection and radiative zones and its amplification to super-equipartition values; Gilman & Rempel (2005) studied how quenching can contribute to the generation of strong super-equipartition fields at the bottom of the convection zone, even if one accounts for the magnetic feedback on differential rotation; and Guerrero et al. (2009) studied the combined effect of diffusivity quenching and poloidal source quenching finding that although diffusivity quenching leads to magnetic field amplification, it also produces solutions which are farther from observations than those of standard kinematic simulations.

In this study, we continue the work in progress presented by Muñoz-Jaramillo et al. (2008) and apply for the first time diffusivity quenching to actual MLT values thanks to current improvements in computational techniques (Hochbruck & Lubich 1997; Hochbruck et al. 1998; Muñoz-Jaramillo et al. 2009).

We focus on two very specific issues that have never been addressed before.

1. Does introducing magnetic quenching of the diffusivity allow the dynamo to reach viable oscillatory solutions if one starts from an MLT estimated profile?

2. Is there any justification for using kinematic diffusivity profiles vis-á-vis the effective turbulent diffusivity after taking quenching into account?

4. THE KINEMATIC MEAN-FIELD DYNAMO MODEL

Our model is based on the axisymmetric dynamo equations:

$$\frac{\partial A}{\partial t} + \frac{1}{s}[\mathbf{v}_p \cdot \nabla(sA)] = \eta\left(\nabla^2 - \frac{1}{s^2}\right)A$$

$$\frac{\partial B}{\partial t} + s\left[\mathbf{v}_p \cdot \nabla\left(\frac{B}{s}\right)\right] + (\nabla \cdot \mathbf{v}_p)B = \eta\left(\nabla^2 - \frac{1}{s^2}\right)B$$

$$+ s\left([\nabla \times (A\hat{\mathbf{e}}_\phi)] \cdot \nabla\Omega\right) + \frac{1}{s}\frac{\partial\eta}{\partial r}\frac{\partial(sB)}{\partial r} + \frac{1}{sr^2}\frac{\partial\eta}{\partial\theta}\frac{\partial(sB)}{\partial\theta}, \quad (3)$$

where A is the ϕ-component of the potential vector (from which B_r and B_θ can be obtained), B is the toroidal field (B_ϕ), v_p is the meridional flow, Ω is the differential rotation, η is the turbulent magnetic diffusivity, and $s = r\sin(\theta)$. In order to integrate these equations, we need to prescribe four ingredients: meridional flow, differential rotation, poloidal field regeneration mechanism, and turbulent magnetic diffusivity. We use the same meridional flow profile defined by Muñoz-Jaramillo et al. (2009), which better captures the features present in helioseismic data. Our flow profile has a penetration depth of 0.675 $R_\odot$ and a top speed of 15.0 m s^{-1}. For the differential rotation we use the analytical form of Charbonneau et al. (1999), with a tachocline centered at 0.7 $R_\odot$ and whose thickness is 0.05 $R_\odot$. For the poloidal field regeneration mechanism, we use the improved ring-duplet algorithm described by Muñoz-Jaramillo et al. (2010) and Nandy et al. (2010), but using a value of $K_0 = 3900$, in order to ensure supercriticality. As Muñoz-Jaramillo et al. (2010), we restrict active region (AR) emergence to latitudes between 45°N and 0°S since observations show that active latitudes are located only within this range (Tang et al. 1984; Wang & Sheeley 1989). Specifics about our treatment of the turbulent diffusivity and numerical methods are described below. More details regarding kinematic dynamo models can be found in a review by Charbonneau (2010) and references therein.

4.1. Turbulent Magnetic Diffusivity and Diffusivity Quenching

As opposed to previous works in which diffusivity is quenched instantly (Tobias 1996; Gilman & Rempel 2005; Muñoz-Jaramillo et al. 2008; Guerrero et al. 2009), we introduce an additional state variable η_{mq}, in order to study the effect of magnetic quenching on dynamo models, governed by the following differential equation:

$$\frac{\partial\eta_{mq}}{\partial t} = \frac{1}{\tau}\left(\frac{\eta_{\mathrm{MLT}}(r)}{1 + \mathbf{B}^2(r, \theta, t)/B_0^2} - \eta_{mq}(r, \theta, t)\right). \quad (4)$$

This treatment allows for an efficient implementation in the context of our numerical scheme (described in Muñoz-Jaramillo et al. 2009), but has at its core the quenching form used by Gilman & Rempel (2005), Muñoz-Jaramillo et al. (2008), and Guerrero et al. (2009), which depends on the magnetic energy in reference to its equipartition counterpart. This has been found to describe the suppression of turbulent diffusivity by MHD simulations (Yousef et al. 2003).

In a steady state, η_{mq} corresponds to the MLT estimated diffusivity $\eta_{\mathrm{MLT}}(r)$ quenched in such a way that the diffusivity
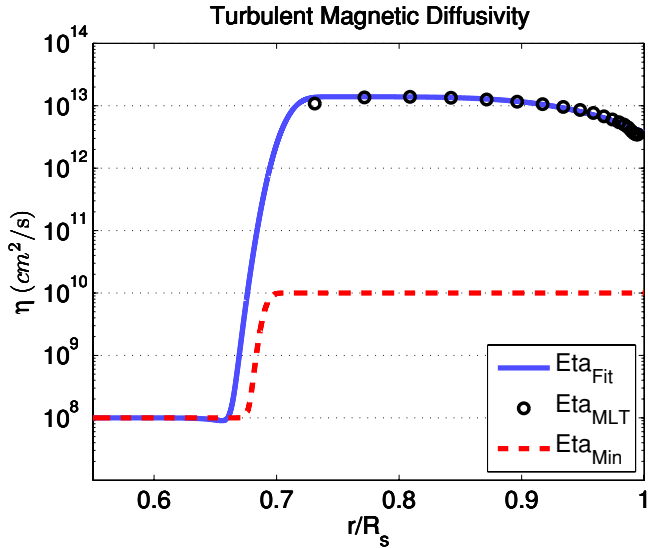
Turbulent Magnetic Diffusivity

Figure 2. Fit (solid line) of diffusivity as a function of radius to the mixing-length theory estimate (circles). As part of our definition of effective diffusivity we put a limit on how much can the diffusivity be quenched. This minimum diffusivity has a radial dependence that is shown as a red dashed line.

(A color version of this figure is available in the online journal.)

is halved for a magnetic field of amplitude $B_0 = 6700$ Gauss (G). This value corresponds to the average equipartition field strength inside the SCZ calculated using the Solar Model S. The average eddy turnover time in the SCZ calculated using Solar Model S corresponds to $\tau = 30$ days. Therefore, the dynamical effect of a magnetic field will be felt locally over this characteristic timescale. For comparison, we also performed simulations using $\tau = 20$ days and $\tau = 10$ days and did not find any major differences in the results. This is to be expected because this timescale is negligible compared to the dynamo cycle period.

We make a fit of $\eta_{MLT}(r)$ using the following analytical profile (see Figure 2):

$$\eta(r) = \eta_0 + \frac{\eta_1 - \eta_0}{2}\left(1 + \mathrm{erf}\left(\frac{r - r_1}{d_1}\right)\right)$$
$$+ \frac{\eta_2 - \eta_1 - \eta_0}{2}\left(1 + \mathrm{erf}\left(\frac{r - r_2}{d_2}\right)\right), \quad (5)$$

where $\eta_0 = 10^8$ cm^2 s^{-1} corresponds to the diffusivity at the bottom of the computational domain; $\eta_1 = 1.4 \times 10^{13}$ cm^2 s^{-1} and $\eta_2 = 10^{10}$ cm^2 s^{-1} control the diffusivity in the convection zone; $r_1 = 0.71\,R_\odot$, $d_1 = 0.015\,R_\odot$, $r_2 = 0.96\,R_\odot$, and $d_2 = 0.09\,R_\odot$ characterize the transitions from one value of diffusivity to another. With this in mind, we define the effective diffusivity at any given point as

$$\eta_{eff}(r, \theta, t) = \eta_{min}(r) + \eta_{mq}(r, \theta, t), \quad (6)$$

with the minimum magnetic diffusivity $\eta_{min}(r)$ given by the following analytical profile (see Figure 2):

$$\eta_{min}(r) = \eta_0 + \frac{\eta_{cz} - \eta_0}{2}\left(1 + \mathrm{erf}\left(\frac{r - r_{cz}}{d_{cz}}\right)\right), \quad (7)$$

where $\eta_{cz} = 10^{10}$ cm^2 s^{-1}, $r_{cz} = 0.69\,R_\odot$, and $d_{cz} = 0.07\,R_\odot$. Since diffusivity is now a state variable, small errors can lead to negative values of diffusivity, which in turn lead to

unbound magnetic field growth. By putting a limit on how small can the diffusivity become, we successfully avoid this type of computational instability. Note that Guerrero et al. (2009) find pervasive small-scale structures for diffusivities lower than 10^9 cm^2 s^{-1} which we avoid by placing this lower limit.

5. DYNAMO SIMULATIONS

We use the SD-Exp4 code (see the Appendix of Muñoz-Jaramillo et al. 2009) to solve the dynamo equations (Equation (3)). Our computational domain comprises the SCZ and upper layer of the solar radiative zone in the northern hemisphere ($0.55\,R_\odot \leqslant r \leqslant R_\odot$ and $0 \leqslant \theta \leqslant \pi$). In order to approximate the spatial differential operators with finite differences we use a uniform grid (in radius and co-latitude), with a resolution of 400×400 grid points.

Our boundary conditions assume that the toroidal and radial magnetic fields are anti-symmetric and the co-latitudinal field is symmetric across the equator ($\partial A/\partial\theta|_{\theta=\pi/2} = 0$; $B(r, \pi/2) = 0$), that the plasma below the lower boundary is a perfect conductor ($A(r = 0.55\,R_\odot, \theta) = 0$; $\partial(rB)/\partial r|_{r=0.55\,R_\odot} = 0$), that the magnetic field is axisymmetric ($A(r, \theta = 0) = 0$; $B(r, \theta = 0) = 0$), and that the field at the surface is radial ($\partial(rA)/\partial r|_{r=R_\odot} = 0$; $B(r = R_\odot, \theta) = 0$). Our initial conditions consist of a large toroidal belt and no poloidal component. After setting up the problem we let the magnetic field evolve for 200 years allowing the dynamo to reach a stable cycle.

6. RESULTS AND DISCUSSION

The first important result is the existence of a uniform cycle in dynamic equilibrium. The presence of diffusivity quenching allows the dynamo to become viable in a regime in which kinematic dynamo models cannot operate, thanks to the creation of pockets of relatively low magnetic diffusivity (where long lived magnetic structures can exist). This can be clearly seen in Figure 3, which shows snapshots of the effective turbulent diffusivity and the toroidal and poloidal components of the magnetic field at different moments during the sunspot cycle (half a magnetic cycle). As expected the turbulent diffusivity is strongly suppressed by the magnetic field (especially by the toroidal component), increasing the diffusive timescale to the point where diffusion and advection become equally important for flux transport dynamics. This slowdown of the diffusive process is crucial for the survival of the magnetic cycle since it gives differential rotation more time to amplify the weak poloidal components of the magnetic field into strong toroidal belts, while providing them a measure of isolation from the top ($r = R_\odot$) and polar ($\theta = 0$) boundary conditions ($B = 0$).

6.1. Spatiotemporal Averages of the Effective Diffusivity

Given that we ultimately want to understand how adequate current kinematic diffusivity profiles are and whether they are plausible representations of physical reality consistent with MLT, we seek to explore the connection between kinematic profiles and the dynamically quenched diffusivity. Because of this, the next natural step is to find spatiotemporal averages of the effective diffusivity. For this purpose we use the generalized mean:

$$\eta_{av}(r_i) = M_p = \left(\frac{1}{N_\theta N_t}\sum_j\sum_n \eta_{eff}(r_i, \theta_j, t_n)^p\right)^{1/p}, \quad (8)$$
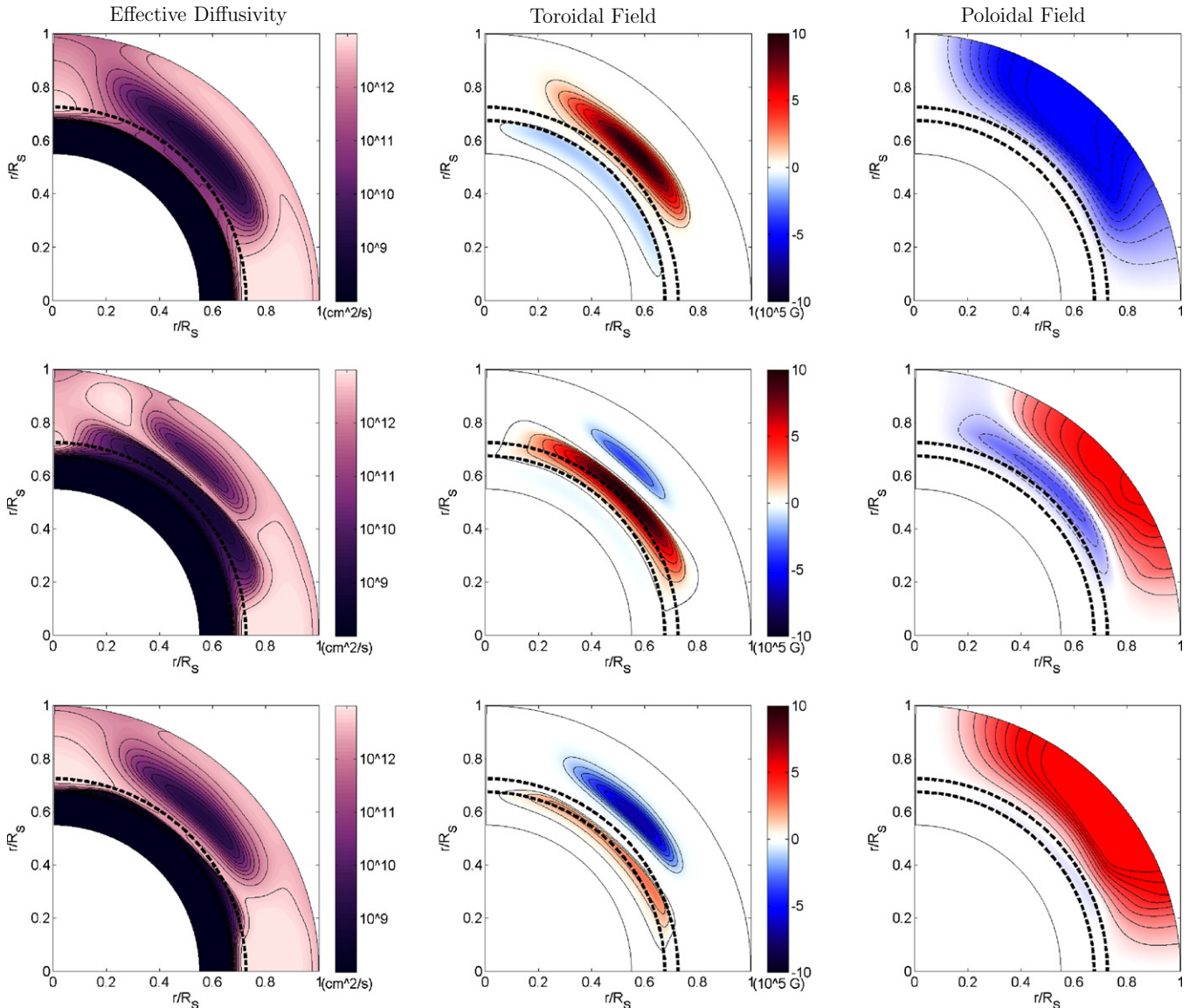
Figure 3. Snapshots of the effective diffusivity and the magnetic field over half a dynamo cycle (a sunspot cycle). For the poloidal field, a solid (dashed) line corresponds to clockwise (counterclockwise) poloidal field lines. Each row is advanced in time by a sixth of the dynamo cycle (a third of the sunspot cycle), i.e., from top to bottom $t = 0$, $\tau/6$, $\tau/3$, and $\tau/2$. As expected, the turbulent diffusivity is strongly depressed by the magnetic field (especially by the toroidal component). This reduces the diffusive timescale to a point where the magnetic cycle becomes viable and sustainable.

(A color version of this figure is available in the online journal.)

where p controls the relative importance given to high orders of magnitude ($p > 0$) and low orders of magnitude ($p < 0$) of the diffusivity. From this generalized mean one can obtain the most commonly used averages: $p \to \infty$ yields the maximum value, $p = 1$ the algorithmic average, $p \to 0$ the geometric average, $p = -1$ the harmonic average, and $p \to -\infty$ the minimum value. The results of calculating these averages are shown in Figure 4(a). Note that one can also obtain temporal averages in which the effective diffusivity depends both on radius and latitude. However, these averages cannot be related to the commonly used kinematic profiles which are exclusively radial. Because of this, we leave the analysis and study of such averages for future work.

6.2. Comparison with Kinematic Dynamo Simulations

Once we calculate the spatiotemporal averages of the effective diffusivity we obtain radial diffusivity profiles that can be used in kinematic dynamo simulations, leaving all other ingredients

intact, in order to compare their solutions with those of the dynamically quenched simulation. We find that the geometric average ($p \to 0$; also known as logarithmic average) shown in Figures 4(a) and (b) as solid lines captures best the essence of the diffusive transport by striking a balance between high- and low-order values of the diffusivity. Interestingly, this average can be accurately described as a double-step profile (Equation (5)) with the following parameters: $\eta_0 = 10^8$ cm² s⁻¹, $\eta_1 = 1.6 \times 10^{11}$ cm² s⁻¹, $\eta_2 = 3.25 \times 10^{12}$ cm² s⁻¹, $r_1 = 0.71\,R_\odot$, $d_1 = 0.017\,R_\odot$, $r_2 = 0.895\,R_\odot$, and $d_2 = 0.051\,R_\odot$ (see circles in Figure 4(b)).

In order to compare the general properties of both simulations we cast the results in the shape of synoptic maps (also known as butterfly diagrams) as can be seen in Figure 5. The results obtained using the MLT estimate and diffusivity quenching (Figure 5(a)) and the results obtained using a conventional kinematic simulation with the geometric average fit (Figure 5(b)) are remarkably similar given the different nature of the two
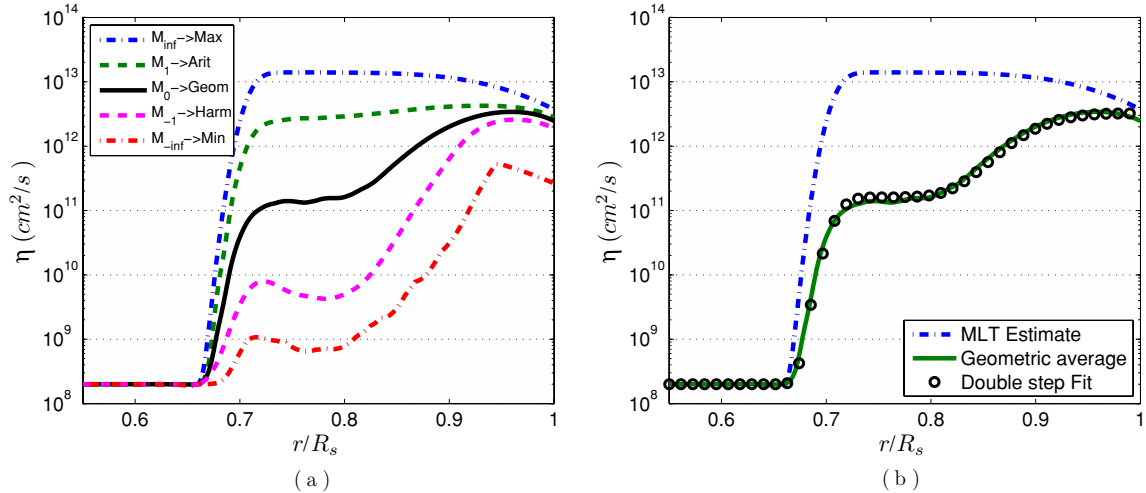
Figure 4. Spatiotemporal averages of the effective diffusivity (a). We find that the geometric time average (b) captures the essence of diffusivity quenching the best.

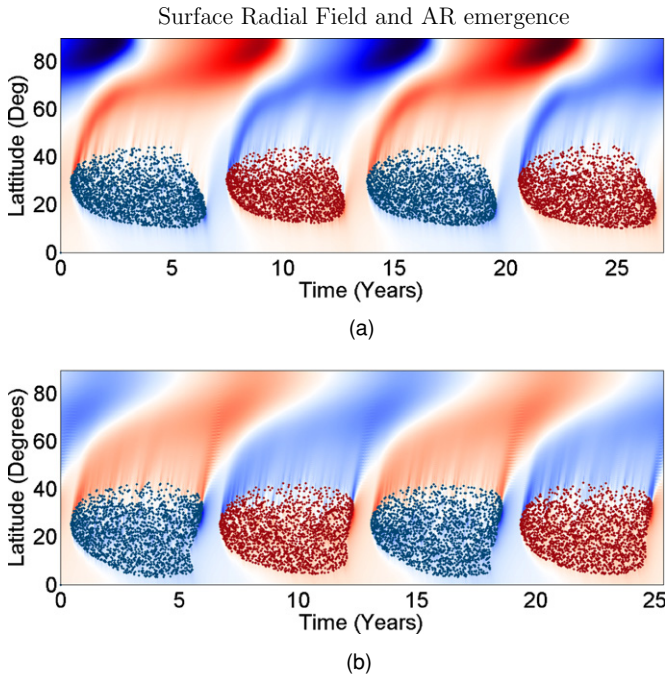(A color version of this figure is available in the online journal.)

Figure 5. Synoptic maps (butterfly diagrams) showing the time evolution of the magnetic field in a simulation using the mixing-length theory (MLT) estimate and diffusivity quenching (a), and a kinematic simulation using the geometric spatiotemporal average of the dynamically quenched diffusivity (b). They are obtained by combining the surface radial field and active region emergence pattern. For diffuse color, red (blue) corresponds to positive (negative) radial field at the surface. Each red (blue) dot corresponds to an active region emergence whose leading polarity has positive (negative) flux. In both sets of simulations we restrict the eruption of active regions in latitude as explained in Section 4. We can see that a kinematic dynamo simulation using the geometric spatiotemporal average can capture the most important features of the magnetic cycle produced by the simulation using the MLT estimate and diffusivity quenching (period, amplitude, and phase).

(A color version of this figure is available in the online journal.)

simulations: the shape of the solutions differs mainly in the AR emergence pattern. However, the general properties of the cycle (amplitude, period, and phase) are successfully captured by the geometric average and are essentially the same. It is important to mention that in these simulations we have not taken into account the feedback of the magnetic field on the global velocity flows

(meridional circulation and differential rotation). This feedback can arise due to direct Lorenz force feedback on the flow fields (Rempel 2006a) and/or magnetic quenching of the turbulent viscosity (which in turn can affect angular momentum transfer; Rempel 2006b). Direct Lorenz force feedback has not been found to have a strong impact on the interaction of the magnetic field with meridional flow, but it does affect toroidal field generation through the reduction of rotational shear (Rempel 2006a); on the other hand turbulent viscosity quenching has been found to alter the meridional flow pattern (Rempel 2006b). Ultimately, both diffusivity quenching and magnetic feedback on the global flow patterns need to be taken into account in order to have a complete picture. Nevertheless, this work defines a framework which can be used to find a physically meaningful diffusivity profile based upon theory and models of the solar interior rather than through heuristic approaches.

6.3. Comparison with Solar Cycle Observations

Ultimately, the goal of dynamo models is to understand the solar magnetic cycle and reproduce and predict its main characteristics. It is therefore important to compare our results with solar observations. It is clear that the solutions are not as successful in reproducing solar characteristics as those of kinematic dynamo simulations whose parameters have been finely tuned: cycle period of seven years instead of eleven, broad wings, and a slight mismatch between the observed and simulated phases of the peak polar field. Guerrero et al. (2009) also find this issue in their simulations, pointing out that the problem may reside in the functional form of diffusivity quenching. Unfortunately, recent MHD simulations attempting to find the validity of the functional form shown in Equation (4) have obtained inconclusive results (Käpylä & Brandenburg 2009). It is clear that additional work is required in order to fully reconcile diffusivity quenching with cycle observations. However, the solutions we obtain are reasonably accurate, given the fact that we have refrained from doing any fine tuning, limiting ourselves to fundamental theories and models.

7. CONCLUSIONS

In summary, we have shown that coupling magnetic quenching of turbulent diffusivity with the estimated profile from MLT allows kinematic dynamo simulations to produce

solar-like magnetic cycles, which was not achieved before. Therefore, we have reconciled MLT estimates of turbulent diffusivity with kinematic dynamo models of the solar cycle. Furthermore, we have demonstrated that kinematic simulations using a prescribed diffusivity profile based on the geometric average of the dynamically quenched turbulent diffusivity are able to reproduce the most important cycle characteristics (amplitude, period, and phase) of the non-kinematic simulations. Incidentally, this radial profile can be described by a double-step profile, which has been used extensively in recent solar dynamo simulations. Although using this profile does not yield solutions as close to solar observations as do finely tuned profiles and the combined effect of diffusivity quenching and magnetic feedback on the global flows still needs to be explored, our approach paves the way for reconciling MLT with kinematic dynamo models.

REFERENCES

Abbett, W. P., Beaver, M., Davids, B., Georgobiani, D., Rathbun, P., & Stein, R. F. 1997, ApJ, 480, 395
Chan, K. L., & Sofia, S. 1987, Science, 235, 465
Charbonneau, P. 2010, Living Rev. Sol. Phys., 7, 3
Charbonneau, P., Christensen-Dalsgaard, J., Henning, R., Larsen, R. M., Schou, J., Thompson, M. J., & Tomczyk, S. 1999, ApJ, 527, 445
Chatterjee, P., Nandy, D., & Choudhuri, A. R. 2004, A&A, 427, 1019
Choudhuri, A. R., Chatterjee, P., & Jiang, J. 2007, Phys. Rev. Lett., 98, 131103
Choudhuri, A. R., Nandy, D., & Chatterjee, P. 2005, A&A, 437, 703
Christensen-Dalsgaard, J., et al. 1996, Science, 272, 1286
Dikpati, M., Corbard, T., Thompson, M. J., & Gilman, P. A. 2002, ApJ, 575, L41
Dikpati, M., de Toma, G., & Gilman, P. A. 2006, Geophys. Res. Lett., 33, 5102
Dikpati, M., & Gilman, P. A. 2007, Sol. Phys., 241, 1
Dikpati, M., Rempel, M., Gilman, P. A., & MacGregor, K. B. 2005, A&A, 437, 699
Gilman, P. A., & Rempel, M. 2005, ApJ, 630, 615
Guerrero, G., & de Gouveia Dal Pino, E. M. 2007, A&A, 464, 341
Guerrero, G., Dikpati, M., & de Gouveia Dal Pino, E. M. 2009, ApJ, 701, 725
Hochbruck, M., & Lubich, C. 1997, SIAM J. Numer. Anal., 34, 1911
Hochbruck, M., Lubich, C., & Selhofer, H. 1998, SIAM J. Sci. Comput., 19, 1552
Jouve, L., & Brun, A. S. 2007, A&A, 474, 239
Käpylä, P. J., & Brandenburg, A. 2009, ApJ, 699, 1059
Moffat, H. K. 1978, in Magnetic Field Generation in Electrically Conducting Fluids, ed. G. K. Batchelor & J. W. Miles (Cambridge: Cambridge Univ. Press), 174
Muñoz-Jaramillo, A., Nandy, D., & Martens, P. C. 2008, AGU Spring Meeting Abstracts, 41, 9
Muñoz-Jaramillo, A., Nandy, D., & Martens, P. C. H. 2009, ApJ, 698, 461
Muñoz-Jaramillo, A., Nandy, D., Martens, P. C. H., & Yeates, A. R. 2010, ApJ, 720, L20
Nandy, D. 2010, in Magnetic Coupling between the Interior and Atmosphere of the Sun, ed. S. S. Hasan & R. J. Rutten (Berlin: Springer), 86
Nandy, D., & Choudhuri, A. R. 2002, Science, 296, 1671
Nandy, D., Munoz, A., & Martens, P. C. H. 2010, Nature, in press
Prandtl, L. 1925, Math. Mech., 5, 133
Rempel, M. 2006a, ApJ, 647, 662
Rempel, M. 2006b, ApJ, 637, 1135
Roberts, P. H., & Soward, A. M. 1975, Astron. Nachr., 296, 49
Rüdiger, G., Kitchatinov, L. L., Kueker, M., & Schultz, M. 1994, Geophys. Astrophys. Fluid Dyn., 78, 247
Tang, F., Howard, R., & Adkins, J. M. 1984, Sol. Phys., 91, 75
Tobias, S. M. 1996, ApJ, 467, 870
Wang, Y., & Sheeley, N. R., Jr. 1989, Sol. Phys., 124, 81
Wilmot-Smith, A. L., Nandy, D., Hornig, G., & Martens, P. C. H. 2006, ApJ, 652, 696
Yeates, A. R., Nandy, D., & Mackay, D. H. 2008, ApJ, 673, 544
Yousef, T. A., Brandenburg, A., & Rüdiger, G. 2003, A&A, 411, 321